

# Stochastic simulation of chemical reactions with spatial resolution and single molecule detail

Steven S Andrews<sup>1</sup> and Dennis Bray<sup>2</sup>

Department of Zoology, Downing Street, University of Cambridge, Cambridge CB2 3EJ, UK

E-mail: ssandrews@lbl.gov and db10009@cam.ac.uk

Received 10 March 2004

Accepted for publication 14 July 2004

Published 12 August 2004

Online at [stacks.iop.org/PhysBio/1/137](http://stacks.iop.org/PhysBio/1/137)

doi:10.1088/1478-3967/1/3/001

## Abstract

Methods are presented for simulating chemical reaction networks with a spatial resolution that is accurate to nearly the size scale of individual molecules. Using an intuitive picture of chemical reaction systems, each molecule is treated as a point-like particle that diffuses freely in three-dimensional space. When a pair of reactive molecules collide, such as an enzyme and its substrate, a reaction occurs and the simulated reactants are replaced by products. Achieving accurate bimolecular reaction kinetics is surprisingly difficult, requiring a careful consideration of reaction processes that are often overlooked. This includes whether the rate of a reaction is at steady-state and the probability that multiple reaction products collide with each other to yield a back reaction. Inputs to the simulation are experimental reaction rates, diffusion coefficients and the simulation time step. From these are calculated the simulation parameters, including the ‘binding radius’ and the ‘unbinding radius’, where the former defines the separation for a molecular collision and the latter is the initial separation between a pair of reaction products. Analytic solutions are presented for some simulation parameters while others are calculated using look-up tables. Capabilities of these methods are demonstrated with simulations of a simple bimolecular reaction and the Lotka–Volterra system.

 This article has associated online supplementary data files

(Some figures in this article are in colour only in the electronic version)

## Nomenclature

### Abbreviations

RDF radial distribution function (see glossary)  
rms root mean square (see glossary)

### Roman symbols

$D$  mutual diffusion coefficient  
 $D_B$  diffusion coefficient for a B molecule

<sup>1</sup> Present address: Calvin Lab, bldg. 3-130, Physical Biosciences Division, Lawrence Berkeley National Laboratory, 1 Cyclotron Road, Berkeley, CA 94720, USA.

<sup>2</sup> Present address: Department of Anatomy, Downing Street, University of Cambridge, Cambridge CB2 3DY, UK.

$G_s(\Delta x)$	Gaussian with area of 1, mean of 0 and standard deviation of $s$
$g(r)$	radial distribution function
$\text{grn}(r, r', s)$	Green's function for diffusion in a radially symmetric system
$\mathbf{J}_B(\mathbf{r}, t)$	flux of B molecules at position $\mathbf{r}$ and time $t$
$k_0$	rate constant for a zeroth-order reaction
$k_1$	rate constant for a unimolecular reaction
$k_{1,i}$	rate constant for the $i$ th unimolecular reaction of a single species
$k_2$	rate constant for a bimolecular reaction
$l_i$	initial distance of a molecule from a surface
$l_f$	final distance of a molecule from a surface
$\text{Prob}(\dots)$	probability

$\text{prob}(\dots)$	probability density
$p_B(\mathbf{r}, t)$	spatial probability density of a single B molecule at position $\mathbf{r}$ and time $t$
$s$	standard deviation of a Gaussian, or a mutual rms step length
$s_B$	rms step length of a B molecule
$\Delta t$	time step for simulation

#### Greek symbols

$\gamma$	boundary condition coefficient for the Collins and Kimball model
$\phi$	probability of geminate recombination
$\rho_B(\mathbf{r}, t)$	number concentration of B molecules at position $\mathbf{r}$ and time $t$
$\sigma_b$	binding radius
$\sigma_u$	unbinding radius

#### Subscripts

$C$	Collins and Kimball model
$N$	Numerical algorithm
$S$	Smoluchowski model, which is also the continuous time model system
$a$	activation limited
$i$	irreversible bimolecular reaction
$r$	reversible bimolecular reaction

## 1. Introduction

Computer simulations can be valuable tools for investigating chemical reaction networks, such as the complex biochemical networks that make up living systems [1–3]. They are best seen as aids to intuition, allowing one to explore the complex dynamics of reaction networks with relative ease. An aspect of this is that a simulation can rigorously determine if a proposed reaction mechanism is consistent with observed results. To mention a few examples, simulations of the *Escherichia coli* chemotaxis signaling network have yielded insights into biological robustness [4], bacterial individuality [5] and protein allostery [6].

Reaction network simulations can be classified by (i) whether they account for spatial information and (ii) whether they include the stochasticity that arises from discrete molecules rather than continuous chemical concentrations. With greater levels of detail, the results become more accurate but the simulations take longer to execute and require more experimental parameters. The algorithms presented in this work are in the most detailed category of this classification scheme, accounting for both stochastic and spatial information. This high level of accuracy is applicable to a wide range of systems but is especially useful for biology, where there can be a high degree of spatial organization [7, 8] and key molecular species often exist with low copy numbers [5, 9]. As an example, a reaction network that includes membrane ion channels is highly sensitive to the stochasticity that arises from individual molecules and spatial influences.

The drawbacks of the high level of detail were reduced as much as possible by designing the algorithms to be computationally efficient and to require few parameters.

The fundamental processes for which algorithms are presented are as follows: molecular diffusion, interactions of molecules with surfaces, zeroth-order chemical reactions (the spontaneous introduction of new molecules into the system, which is physically impossible but computationally useful), unimolecular chemical reactions and bimolecular chemical reactions. In all but the last case, the algorithms yield results that are in exact accord with those of a simplified model system. However, achieving the same accuracy for bimolecular reactions would make a simulation too slow to be useful. Instead, we present a fast alternative method and show that it yields results in good agreement with analytical models.

Our algorithms have been implemented in a C language computer program called *Smoldyn* (for *Smoluchowski dynamics*) which may be downloaded from the World Wide Web. Another publicly available computer program that works at a similar level of detail is *MCell*, which was originally developed to model signaling in neuromuscular junctions [10], although it works at a lower level of spatial resolution and it has the limitation that bimolecular reactions can only be simulated at surfaces.

## 2. The model system

In this section, real chemical processes are simplified to a precisely defined model system. Our model is an extension of the *Smoluchowski model* for *diffusion-influenced* systems [11], which is presented here as well.

In the model, time increases continuously, as it does in nature, but in contrast to the finite time steps that are introduced in the next section for the simulation algorithms. Each molecule is treated as a point-like particle that diffuses freely in space with continuously variable  $x$ ,  $y$  and  $z$  coordinates, quantified with Fick's laws [12]:

$$\mathbf{J}_B(\mathbf{r}, t) = -D_B \nabla \rho_B(\mathbf{r}, t) \quad (1)$$

$$\dot{\rho}_B(\mathbf{r}, t) = D_B \nabla^2 \rho_B(\mathbf{r}, t). \quad (2)$$

$B$  is some generic chemical species,  $\mathbf{J}_B(\mathbf{r}, t)$  is the flux of  $B$  molecules at position  $\mathbf{r}$  and time  $t$ ,  $\rho_B(\mathbf{r}, t)$  is the local number concentration of  $B$  molecules, and  $D_B$  is the diffusion coefficient for  $B$  [13]. The coordinates of a molecule are its center of mass. The Smoluchowski description also accounts for external and long-range forces (such as between ionic species [14]) but we ignore them because they have minimal influence in a typical biochemical system and they are computationally expensive to simulate. To allow the use of Fick's laws on small size scales as well as large ones, the dynamics of the solvent and other unreactive species are ignored [15], leading to infinitely detailed *Brownian motion* of the reactive molecules. This approximation makes the results only accurate on size scales that are somewhat larger than those of individual molecules. Similarly, steric interactions are ignored between molecules that do not react with each other, which is valid for dilute solutions. Molecular spatial

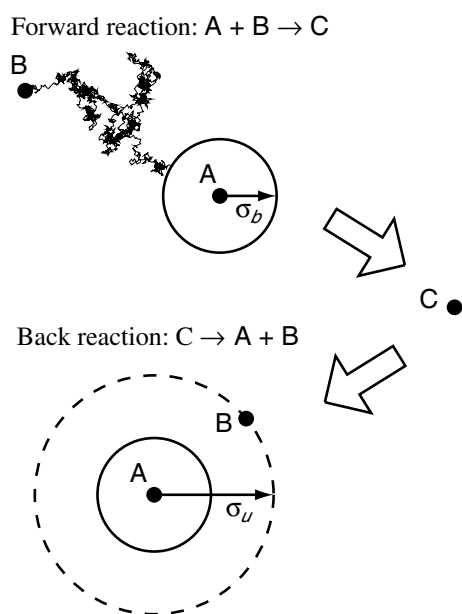


**Figure 1.** Forward and back reactions in the physical model for the reaction  $A + B \leftrightarrow C$ , shown from the standpoint of an A molecule. A forward reaction occurs when the centers of an A and a B molecule (black dots) diffuse to a separation that is equal to the binding radius,  $\sigma_b$  (circle with solid line), forming a C molecule. When a back reaction occurs, the A and B products are initially separated by the unbinding radius,  $\sigma_u$  (circle with dashed line), which is made larger than the binding radius so as to prevent the instant recombination of the products. The angular location of B is random due to rotational diffusion. The same method is used for the numerical algorithms presented in this paper although, for computational efficiency, diffusion is simulated with relatively long steps and the sizes of the binding and unbinding radii are modified so as to yield quantitatively accurate reaction rates.

orientations and internal energy levels typically fluctuate on time scales that are faster than the diffusive and reactive processes that are of interest [14, 16], allowing them to be ignored as well. Because of these approximations, the complete time-dependent state of the model is fully specified by a list of the molecular positions.

By definition, a *diffusion-limited* bimolecular reaction occurs very rapidly once two reactive molecules come into contact, which happens when the molecular centers are separated by a distance equal to the sum of the molecular radii. This description is used for the Smoluchowski model in which a bimolecular reaction occurs at the moment when two reactive molecules collide with each other. Smoluchowski derived the steady-state reaction rate for this physical description, in terms of the molecular radii and the diffusion coefficients [11]. However, most reactions occur at a slower rate because of a reaction activation energy. This is addressed in the Smoluchowski model by replacing the sum of the molecular radii with a smaller effective *binding radius* ( $\sigma_b$ ), thus yielding the correct steady-state reaction rate for all bimolecular reactions, regardless of the reaction mechanism (see figure 1). This binding radius is derived below.

Reversible reactions, such as the generic reaction  $A + B \leftrightarrow C$ , pose a problem. If the A and B products of the

backward reaction are initially separated by the binding radius, which is the obvious separation, then the ensuing Brownian motion of A and B makes them almost certain to collide again. This leads to a nearly instantaneous reaction back to C, which is clearly not acceptable. (The terms ‘almost’ and ‘nearly’ are understatement since the actual probability for recollision is 1 and the expected time that elapses before reacting is 0 [17]. Qualitatively, an initial separation of  $\sigma_b$  implies that any net motion of the molecules towards each other yields a reaction, which is nearly certain because true Brownian motion has an infinite number of random walk steps in a finite time period; all but a vanishingly small portion of the possible random walks include at least a little net motion of the molecules towards each other.) This recollision problem is not addressed in the Smoluchowski model because it does not consider reversible reactions. The related *Collins and Kimball model* solves the problem by replacing the rule that reactions always occur upon collision with one in which there is a certain probability of a reaction at each collision [17, 18]. While useful mathematically, this confuses the physical picture because a single collision almost certainly leads to infinitely more collisions, implying that the probability of reaction at each collision must be infinitesimal. For ease of simulation, our scheme is closer to the spirit of the Smoluchowski model: the A and B dissociation products are initially separated by a fixed distance which is larger than  $\sigma_b$ , called the *unbinding radius* ( $\sigma_u$ ) [19]. Using this rule, neither inter-molecular forces nor reaction probabilities need to be introduced, leaving diffusion as the sole fundamental process. After unbinding, the A and B product molecules may diffuse away from each other or they may diffuse together again and rebind, called a *geminate recombination* [14, 20].

An unbinding radius is an artificial concept but its use can be justified. Physically, a C molecule is an A–B complex, for which the interaction potential energy is a function of the A–B separation, typically with an activation barrier [21]. If diffusion influences the system even a small amount, any boundary between reactants and products may be crossed many times. To prevent this, it is helpful to introduce bistability by defining a boundary on each side of the activation barrier: a forward reaction occurs when the A–B separation is less than the inner boundary and a reverse reaction occurs when it is greater than the outer boundary [22]. The model defined here does not have an activation barrier, although we retain the two boundaries.

Most aspects of this model on size scales of individual molecules or smaller are incorrect, such as infinitely detailed Brownian motion, the assumption that molecules do not have excluded volume, and reaction dynamics with fixed binding and unbinding radii. However, all aspects of the model are qualitatively correct on larger size scales because macroscopic diffusion does follow Fick’s laws and reactions only occur between physically proximate molecules. It becomes quantitatively accurate when the model is supplemented with experimental data, including diffusion coefficients and reaction rates.

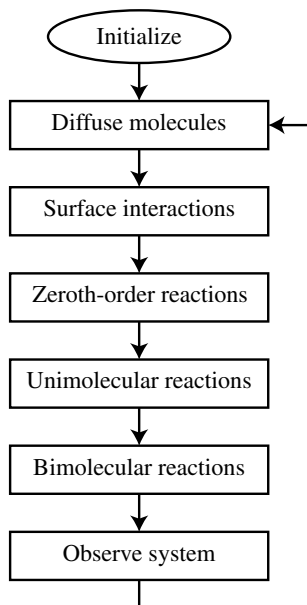


**Figure 2.** Flowchart for our simulation program *Smoldyn*. Alternating diffusion and bimolecular reactions are an essential aspect of the bimolecular reaction algorithm.

### 3. Simulation algorithms

In this section, the model is converted from a simplified description of physical processes to numerical algorithms. To do this, the continuous time of the model is replaced with steps of length  $\Delta t$ , which can be kept constant throughout the simulation [23] (which is done in *Smoldyn*) or made adaptive so as to focus computational effort on important time segments [24]. Either way, it is helpful to think of the end of each step as an observation of a virtual system that evolves continuously. In particular, molecules are considered to move with infinitely detailed Brownian motion, even though the detail is neither explicitly simulated nor observable. Using this interpretation, these algorithms are designed to yield observable results that are as close as possible to the analytically derived dynamics of the model system. The simulation errors can be made arbitrarily small because the simulated dynamics become identical to those of the model in the limit of small time steps. Except for the bimolecular reaction one, each algorithm can be called ‘exact’ because the simulated results are also identical to those of the model for arbitrarily long time steps in the absence of coupling with other processes.

A conventional program framework is used here, in which the program has some initialization procedures and then runs a loop over time steps (figure 2). During each iteration of the loop, several processes are simulated independently, described below in turn. See appendix A for implementation details.

#### 3.1. Molecular diffusion

Because the model considers individual molecules rather than concentrations, Fick’s second law (equation (2)) is rewritten as a master equation by replacing the number density of B

molecules with the spatial probability density for a single molecule:

$$\dot{p}_B(\mathbf{r}, t) = D_B \nabla^2 p_B(\mathbf{r}, t) \quad (3)$$

The product  $p_B(\mathbf{r}, t) d\mathbf{r}$  is the probability that a specific B molecule is within volume  $d\mathbf{r}$  about position  $\mathbf{r}$  at time  $t$ . In a simulation, a molecule starts at a known position and diffuses over the course of a time step. Solving equation (3) for this initial condition shows that the probability density for the displacement of a molecule after a time step has a Gaussian profile on each Cartesian coordinate [12, 25]:

$$p_B(\mathbf{r} + \Delta\mathbf{r}, t + \Delta t) = G_{s_B}(\Delta x) G_{s_B}(\Delta y) G_{s_B}(\Delta z) \quad (4)$$

$$G_s(\Delta x) \equiv \frac{1}{s\sqrt{2\pi}} \exp\left(-\frac{\Delta x^2}{2s^2}\right) \quad (5)$$

$$s_B \equiv \sqrt{2D_B \Delta t} \quad (6)$$

where  $\Delta x$ ,  $\Delta y$  and  $\Delta z$  are the Cartesian displacements,  $G_s(\Delta x)$  is a normalized Gaussian with mean 0 and standard deviation equal to  $s$ , and  $s_B$  is the *root mean square (rms) step length* of species B. These results form the basis of a simulation method called *Brownian dynamics* [26, 27] in which diffusion is simulated by picking a normally distributed random displacement for each molecule at each time step.

#### 3.2. Treatment of surfaces

Nearly all physical reaction systems are confined to a finite volume, making it necessary to simulate surface interactions. Surfaces are most easily treated as arrays of flat panels which might be as simple as the square walls of a cubical reaction volume or as complex as the membranes of a neuromuscular junction [10]. From a computational viewpoint, surface types include the following: inert impermeable surfaces, which prevent molecules from passing from one side to the other; periodic boundaries of the simulation volume (also called toroidal boundaries), which do not exist physically but are useful for the simulation of systems with effectively infinite extent; and absorbing surfaces, which irreversibly capture all molecules that diffuse into them. In each case, the algorithm has to determine whether each molecule interacted with each panel of the surface during the previous time step using the standard criterion that all observable dynamics should be indistinguishable from those of the model.

Impermeable surfaces are considered first. Solving equation (3) with an impermeable plane as a boundary condition shows that the spatial probability density,  $p_B(\mathbf{r}, t)$ , reflects off the surface like light from a mirror [25]. Thus, even though molecules are assumed to move exclusively by Brownian motion over the course of a time step and the surface may be quite rough on a microscopic scale, diffusion in the presence of inert impermeable surfaces is accurately simulated using ballistic-type reflections [26]. In the algorithm, each molecule is propagated forward over  $\Delta t$  according to equation (4); then, the straight line path of the molecule is reflected off any surface that it crosses.

Periodic boundaries are similar. Because equation (4) is correct in the absence of surfaces, it is also correct for

periodic boundaries, provided that any probability density that escapes the system is translated across the simulation volume. In the algorithm, any molecule that diffuses past a boundary is transferred across the system as though it had followed a straight line over the course of the time step.

An absorbing surface is treated by temporarily considering it to be permeable and asking the question: what is the probability that a specific molecule crossed the surface during the time step? If the molecule started on the inside and diffused to the outside, then it obviously crossed the surface and should be absorbed. It could also start and end on the inside but have crossed the surface during the time step, the probability of which can be found using the initial and final perpendicular distances to the surface, denoted by  $l_i$  and  $l_f$ , respectively (these are positive if the molecule is inside and negative if it is outside). The probability that the molecule crossed the surface at least once, starting from distance  $l_i$ , conditioned with the additional knowledge of  $l_f$ , is

$$\begin{aligned} \text{Prob}(\text{cross}|l_f) &= 1 - \text{Prob}(\text{no cross}|l_f) \\ &= 1 - \frac{\text{prob}(\text{no cross}, l_f)}{\text{prob}(l_f)}. \end{aligned} \quad (7)$$

$\text{Prob}()$  is a probability,  $\text{prob}()$  is a probability density, a vertical line indicates a conditional probability, and a comma indicates a joint probability [28]. For example,  $\text{Prob}(\text{cross}|l_f)$  is the probability that the boundary is crossed, given a knowledge of  $l_f$ , and  $\text{prob}(\text{no cross}, l_f) dl$  is the probability that the boundary is not crossed and the final distance is between  $l_f$  and  $l_f + dl$ . The densities are found with equation (3) and the initial condition that the molecule starts at  $l_i$  away from a surface [25]. For the joint density, a boundary condition is that the probability that the molecule is at the surface is 0. Results are

$$\text{prob}(\text{no cross}, l_f) = G_{s_B}(l_f - l_i) - G_{s_B}(l_f + l_i) \quad (8)$$

$$\text{prob}(l_f) = G_{s_B}(l_f - l_i). \quad (9)$$

Substituting these into equation (7) yields the desired answer:

$$\text{Prob}(\text{cross}|l_f) = \exp\left(-\frac{2l_i l_f}{s_B^2}\right). \quad (10)$$

Thus, the algorithm for absorbing surfaces is that a molecule should be absorbed if it ends up on the far side of the surface at the end of a time step or if a random number with a uniform distribution between 0 and 1 is less than  $\exp(-2l_i l_f / s_B^2)$ .

All of these methods are exact for planar surfaces but are in error for curved surfaces or near junctions of flat surface panels. An example is a pore in a membrane (figure 3): using the continuous time model, a molecule might curve around after going through the pore, but the diffusion algorithm only allows molecules to travel in straight lines during time steps. In general, the spatial resolution is approximately the molecular rms step length.

### 3.3. Zeroth-order reactions

A zeroth-order reaction progresses at a rate that is independent of all chemical concentrations, implying that product molecules are formed spontaneously. While unphysical, zeroth-order reactions can be useful components

Model: detail is infinite



Simulated: detail ~ rms step length

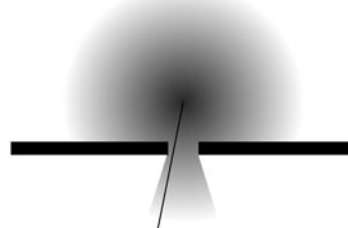


**Figure 3.** Example of limited spatial resolution in the simulation. The top panel shows diffusion through a pore in a membrane (gap in black bar) using the model system. The molecule starts above the pore. The thin black line shows a representative molecule trajectory and the shading represents the probability that the particle ends at each location. The lower panel presents the same information for the simulation, where it is seen that the probability density below the pore is incorrect due to the use of finite length time steps and straight line trajectories. Accurate results would require a shorter time step.

of simulations because they can provide chemical inputs to the simulated system without requiring a complete treatment of the input mechanism. For example, a chemical reactor might have an input port that continuously adds a chemical, or a biological cell may include a protein that is synthesized by biosynthetic pathways that are not of immediate interest. In both cases, these could be treated explicitly, or they could be simulated using a zeroth-order reaction to produce exactly the same result.

If the product of the reaction is A and  $k_0$  is the rate constant, the zeroth-order mass-action rate law is

$$\dot{\rho}_A = k_0. \quad (11)$$

On average,  $k_0 \Delta t$  product molecules are formed during each time step. However, this has some stochastic variation, which is given with a Poisson distribution [28].

### 3.4. Unimolecular reactions

Unimolecular reactions are described by the generic equation  $A \rightarrow \text{products}$ . This might describe a true unimolecular reaction, such as a molecular dissociation, or a bimolecular reaction between an A molecule and an abundant species that is not explicitly simulated. The kinetics are typically of first-order:

$$\dot{\rho}_A = -k_1 \rho_A \quad (12)$$

where  $k_1$  is the first-order rate constant. Upon integration, the probability that a specific A molecule reacts during  $\Delta t$  is

$$\text{Prob}(\text{reaction}) = 1 - \exp(-k_1 \Delta t). \quad (13)$$

If an A molecule can react via multiple first-order pathways, a sequential application of equation (13) leads to a bias towards the first pathway that is attempted. Instead, solution of a collection of equations like equation (12), where the  $i$ th reaction has a first-order rate constant  $k_{1,i}$ , leads to the reaction probabilities [10]:

$$\text{Prob}(\text{reaction } i) = \frac{k_{1,i}}{\sum_j k_{1,j}} \left[ 1 - \exp \left( -\Delta t \sum_j k_{1,j} \right) \right]. \quad (14)$$

The efficient simulation of these equations is discussed in appendix A.

### 3.5. Bimolecular reactions

Bimolecular reactions, described by the generic equation  $A + B \rightarrow C$ , have the steady-state reaction rate:

$$\dot{\rho}_C = k_2 \rho_A \rho_B \quad (15)$$

where  $k_2$  is the second-order rate constant, from which it is possible to find the binding radius of the model. An exact algorithm would be based on a question similar to that posed above for absorbing surfaces: given the positions of molecules A and B before and after a time step, what is the probability that the distance between them was less than the binding radius at some point during the time step? Equations analogous to equations (7) to (10) can be written and solved for this situation (they are derivable from equations presented in chapter 14 of [29]). However, the most simplified result still requires a numerical integral, making it too computationally expensive for simulations. Even a transcription of the result to a look-up table requires a very large table, four-dimensional interpolation (initial separation, final separation, interior angle and binding radius), and still requires many calculations for every potential collision at every time step. Unlike the other algorithms, an exact solution for bimolecular reactions is not practical. However, there may be reasonably efficient simulation methods if one abandons the intuitive representation presented here, along with the option of using constant size time steps [30, 31].

Because of these difficulties, we temporarily ignore the theory and choose an algorithm that is intuitive, simple and very fast: two molecules always react if they end up within  $\sigma_b(\Delta t)$  at the end of a time step and never react if the final separation is greater than that. For reversible reactions, dissociation products are initially separated by  $\sigma_u(\Delta t)$ . These parameters are analogous to the binding and unbinding radii of the model system (figure 1) and approach them in the limit of small time steps. They are derived in the next section and the resulting dynamics are investigated in the following section.

## 4. Bimolecular reaction parameters

The correct binding radius for the simulation is, quite simply, that value which makes the simulated bimolecular reaction rate equal the experimental rate. The latter is presumed known, so we derive the simulated reaction rate in terms of the binding

radius, equate it to the experimental rate constant, and invert the result to yield the binding radius. Unfortunately, the derivation is complicated.

The first complication occurs in deciding which experimental reaction rate to use. As usual, the chemical equation is  $A + B \rightarrow C$ . Suppose we start with a *well-mixed* distribution of reactants, which is one in which the molecules have random positions but with the constraint that no A–B pairs are allowed to be closer than a binding radius of each other. As we observe the subsequent reactions, we see that the reaction rate ‘constant’ given in equation (15) is not actually constant but is extremely high initially, because of A–B pairs that happen to start close to each other, and then decreases and approaches a *steady-state* value [11, 14, 32]. This steady-state value is nearly always the one that is reported as the experimental reaction rate. Thus, our approach is to find the binding radius which makes the simulation, using a steady-state distribution of A and B molecules, reproduce the reported reaction rate. The resulting binding radius is a parameter of the model, so it is equally applicable at steady-state *and* away from steady-state.

In these derivations, separate equations are found for (i) the dynamics that arise from the analytical model that was defined in the section 2 and which is based on Smoluchowski dynamics and (ii) those that arise from the numerical algorithms. In cases where equations differ between the Smoluchowski based model and the numerical algorithm, they are labeled with subscripts ‘S’ and ‘N’, respectively. Additionally, the subscripts ‘i’ and ‘r’ are used to distinguish results for irreversible and reversible reactions. Look-up tables and source code are available as supplementary information<sup>3</sup>, as described at the end of the text.

### 4.1. Irreversible reactions, Smoluchowski model

The *radial distribution function* [33] (RDF,  $g(r)$ ) between A and B molecules is the average distribution of distances between A and B molecules. More precisely,  $\rho_B g(r) dr$  is the probability that there is a B molecule within a small volume element  $dr$  at distance  $r$  from any specific A molecule, where  $\rho_B$  is the overall number density of B. Because A and B molecules react when they collide,  $g(r)$  equals 0 for  $r < \sigma_b$ . Any influence between A and B molecules diminishes for large separations, so  $g(r)$  approaches 1 as  $r$  tends to infinity. While it is conceptually possible to start a chemical system with nearly any shape RDF, the Smoluchowski RDF for irreversible reactions always approaches the steady-state solution [14] (figure 4(A)):

$$g_{Si}(r) = 1 - \frac{\sigma_b}{r}, \quad r > \sigma_b. \quad (16)$$

The depletion of B molecules around A molecules arises not from any long-range interaction, but because reactive species that are close together are likely to react, which excludes them from the average [17].

The reaction rate is the net flux of B molecules towards A molecules, which is calculated using equation (3) and the

<sup>3</sup> Supplementary data files are available from [stacks.iop.org/PhysBio/1/3/001](https://stacks.iop.org/PhysBio/1/3/001).

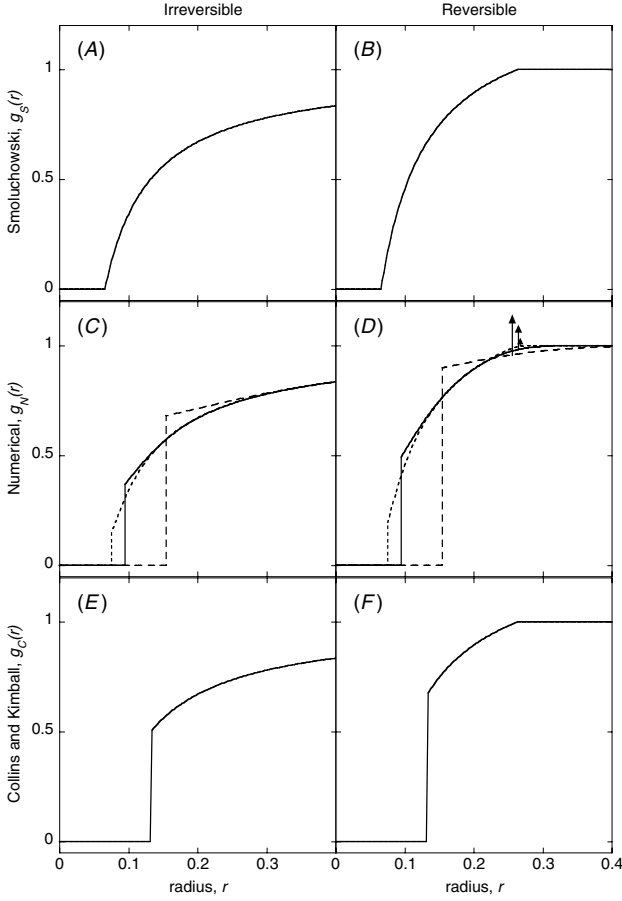


**Figure 4.** Radial diffusion functions (RDFs) for bimolecular reactions at steady-state with various models. Diffusion coefficients are  $10^{-8} \text{ cm}^2 \text{ s}^{-1}$  for each reactant and rate constants are  $10^6 \text{ M}^{-1} \text{ s}^{-1}$  for irreversible reactions. For reversible reactions, geminate recombination probabilities are 0.25 and rate constants are increased to  $1.3 \times 10^6 \text{ M}^{-1} \text{ s}^{-1}$  to account for geminate reactions (equation (28)). (A) Smoluchowski model (equation (16)) with  $\sigma_b = 0.066 \text{ nm}$ . (B) Smoluchowski model (equation (29)) with  $\sigma_b = 0.066 \text{ nm}$  and  $\sigma_u = 0.264 \text{ nm}$ . (C) Numerical algorithm with  $\sigma_b = 0.075 \text{ nm}$ ,  $s = 0.049 \text{ nm}$ ,  $k_{Ni} = 2 \times 10^6 \text{ M}^{-1} \text{ s}^{-1}$ , and  $\Delta t = 0.61 \text{ ns}$  for the solid line; other lines use time steps that are 0.061 and 6.1 ns, shown with short and long dashes, respectively. (D) Lines are the same as those in (C) but for reversible reactions; for the solid line,  $\sigma_u = 0.264 \text{ nm}$ . Arrows represent Dirac delta functions at the unbinding radii. (E) Collins and Kimball model (equation (33)) with  $k_{Ca} = 2 \times 10^6 \text{ M}^{-1} \text{ s}^{-1}$  and  $\sigma_b = 0.132 \text{ nm}$ . (F) Collins and Kimball model (equation (35)) with  $k_{Ca} = 2 \times 10^6 \text{ M}^{-1} \text{ s}^{-1}$ ,  $\sigma_b = 0.132 \text{ nm}$  and  $\sigma_u = 0.264 \text{ nm}$ . Note that the RDF for the numerical algorithm approaches the Smoluchowski RDF for short time steps, a well-mixed RDF (a step function) for long time steps, and is qualitatively similar to that of the Collins and Kimball model.

definition of the RDF. The general reaction rate for models in which time is treated continuously and its solution for the Smoluchowski model at steady-state are, respectively,

$$\dot{\rho}_C = 4\pi\sigma_b^2 D\rho_A\rho_B \left. \frac{\partial g(r)}{\partial r} \right|_{\sigma_b} \quad (17)$$

$$\dot{\rho}_C = 4\pi D\sigma_b\rho_A\rho_B \quad (18)$$

Here  $D$  is the *mutual diffusion coefficient* [34], defined as  $D_A + D_B$ . The proportionality of the reaction rates to  $\rho_A$  and  $\rho_B$  is the same as in the second-order rate equation, leading to the well-known solution of the rate constant for irreversible reactions according to the Smoluchowski model [11]:

$$k_{Si} = 4\pi D\sigma_b. \quad (19)$$

This rate is limited only by diffusion, so  $k_{Si}$  is the diffusion-limited rate constant.

#### 4.2. Irreversible reactions, numerical algorithm

In the limit of short simulation time steps, the diffusion simulated by Brownian dynamics approaches the infinitely detailed Brownian motion that the model assumes. Thus, in this limit, the numerical reaction rate constant,  $k_{Ni}$ , is equal to the Smoluchowski result in equation (19). Solving the equation for  $\sigma_b$ , which is the only necessary simulation parameter (the notation  $\sigma_b(\Delta t)$  was simplified to just  $\sigma_b$ ), yields a solution that is valid whenever the *mutual rms step length* is much smaller than the binding radius; the mutual rms step length is defined as  $s = (2D\Delta t)^{1/2} = (s_A^2 + s_B^2)^{1/2}$ . It is instructive to see when this solution can be used. A typical reaction rate for proteins is  $10^6 \text{ M}^{-1} \text{ s}^{-1}$  and protein diffusion constants are typically at least  $10^{-8} \text{ cm}^2 \text{ s}^{-1}$ . These are substituted into equation (19), and then equation (6) is solved for  $\Delta t$  to yield  $\Delta t \ll 1 \text{ ns}$ . A simulation time step of a nanosecond or longer would not just limit spatial resolution, but would produce a simulation with the incorrect reaction rate. On the other hand, the use of a sufficiently short time step would make most simulations run much too slowly to be useful.

Next, we turn to the long time step limit, given by the condition  $s \gg \sigma_b$ . Now, any correlations between the positions of reactants are eliminated after the simulation executes one iteration of the diffusion algorithm, so the probability that a certain A will react with a certain B is just the ratio of the volume of a sphere of radius  $\sigma_b$  to the total system volume. Multiplying by the numbers of A and B molecules and changing to concentrations yields the numerical rate constant for the long time step limit:

$$k_{Ni} = \frac{4\pi}{3}\sigma_b^3 \Delta t, \quad \Delta t \rightarrow \infty. \quad (20)$$

Using the same reaction rate and diffusion coefficients as above, this equation is not valid until the mutual rms step length is greater than around 100 nm (using  $s = 10\sigma_b$ ). A step length this long precludes the possibility of attaining spatial resolution anywhere near the sizes of molecules, making it not generally useful either.

Between these limits,  $k_{Ni}$  cannot be solved analytically, so it was calculated numerically to create a look-up table for later use (available as supplementary information). The number of variables was minimized by dividing all lengths by the binding radius, leading to unitless variables:  $k_{Ni} \Delta t / \sigma_b^3$  is the reduced reaction rate,  $s' = s / \sigma_b$  is the reduced rms step length, and  $\sigma_b / \sigma_b = 1$  is the reduced binding radius. To perform the calculation, a tabulated RDF (500 equally spaced data points, with reduced radii from 0 to 10) was evolved over time exactly as it would evolve in the simulation algorithm, by alternating

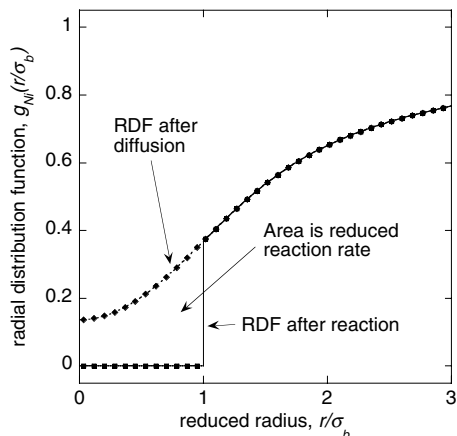


**Figure 5.** Method used for calculating the reduced bimolecular reaction rate,  $k_{Ni} \Delta t / \sigma_b^3$ , for irreversible reactions. A tabulated RDF was alternately integrated with Green's function to simulate diffusion and set to 0 between  $r = 0$  and  $r = 1$  to simulate reactions. After steady-state was reached, the RDF after diffusion (diamonds and dashed line) and the RDF after absorption (squares and solid line) were saved and the area between  $r = 0$  and  $r = 1$  of the former function was integrated to find the reduced reaction rate. Tabulated RDFs for irreversible reactions extended to a reduced radius of 10, while those for reversible reactions extended to  $\sigma_u' + 3$ ; all RDFs used 500 data points (for clarity, only every fifth data point is shown).

diffusion steps and irreversible reaction steps. The calculation began with either the RDF in equation (16) or with  $g(r) = 1$  for all  $r > 1$  and was continued until the RDF converged to a steady-state result (figure 5).

Conceptually, diffusion of an RDF from an initial state to its state after time  $\Delta t$  is computed by convolving the three-dimensional radial distribution function with a three-dimensional Gaussian with standard deviation  $s'$  (analogous to equation (4)). Because of rotational symmetry, this convolution simplifies to the integral of the product of the RDF and the appropriate Green's function [14, 29], given as  $gm(r, r', s)$ :

$$g_{Ni, \text{final}}(r) = \int_0^\infty 4\pi r'^2 gm(r, r', s) g_{Ni, \text{initial}}(r') dr' \quad (21)$$

$$gm(r, r', s) = \frac{1}{4\pi r r'} [G_s(r - r') - G_s(r + r')]. \quad (22)$$

Most of the integral in equation (21) was calculated numerically using the tabulated RDF and the trapezoid method [35]. The rest of the integral, from the end of the tabulated RDF to infinity, was calculated by extrapolating the RDF with a function of the form  $1 + a/r$  which is the general solution of equation (3) with the boundary condition that  $g_{Ni}(r)$  tends to 1 for large  $r$ ;  $a$  is a fitting parameter that was found using the final 10% of the tabulated RDF. The analytic integral for the extrapolated portion, which was then combined with the numerical integral, is

$$\begin{aligned} & \int_{r_1}^\infty 4\pi r'^2 gm(r, r', s) \left(1 + \frac{a}{r'}\right) dr' \\ &= 4\pi s^2 r_1 gm(r, r_1, s) + \frac{1}{2}(e_- + e_+) + \frac{a}{2r}(e_- - e_+) \end{aligned} \quad (23)$$

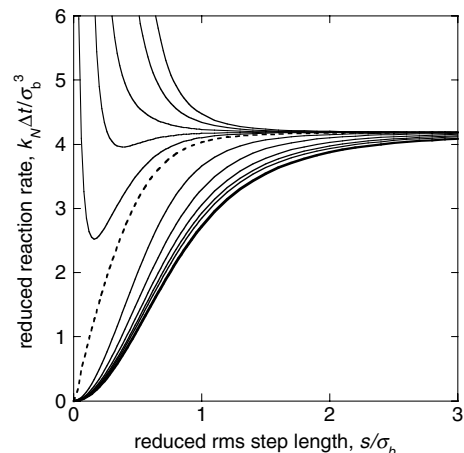


**Figure 6.** The reaction rate for the numerical algorithm as a function of the algorithm parameters, which are the rms step length and binding and unbinding radii. The bold line (lowest line) represents irreversible reactions. From top to bottom, the other lines are for reversible reactions with reduced unbinding radii that are 0, 0.5, 0.7, 0.8, 0.9, 1.0 (dashed line), 1.6, 2.5, 4.0, 6.3 and 10.0. Shown are interpolations and extrapolations from tabulated data, extended with analytical solutions where available.

$$e_\pm \equiv \operatorname{erfc} \frac{r_1 \pm r}{s\sqrt{2}}. \quad (24)$$

After a diffusion step, the reduced reaction rate was computed by numerically integrating the tabulated RDF from 0 to the reduced binding radius (figure 5):

$$\frac{k_{Ni} \Delta t}{\sigma_b^3} = \int_0^1 4\pi r^2 g_{Ni}(r) dr. \quad (25)$$

Afterwards, these values of  $g_{Ni}(r)$  were set to 0 to mimic the reaction portion of the simulation algorithm. The RDF was considered to have achieved steady-state when the reduced rate constant varied by less than 1 part in  $10^5$  over sequential iterations (figure 4(C)).

To improve accuracy and provide an error estimate, the calculation was run in two directions: starting with long rms step lengths, leading to reduced rate constants that decreased asymptotically as steady-state was approached, and vice versa. These results were averaged to yield best estimates for the reduced rate constants. The difference between results was never greater than 5%, implying that calculation errors due to the RDF not being at steady-state are likely to be less than 2.5%. Other potential errors were minimized by increasing the density of data points and the maximum tabulated radius until changes in results were much less than the errors quoted above. Also, it was confirmed that the RDF approached equation (16) for short time steps and a step function for long time steps.

The result of these calculations is the bold line at the bottom of figure 6, produced with a smooth interpolation of the calculated rates. Although the figure is shown with reduced units, this line represents  $k_{Ni}$  as a function of  $\sigma_b$  and  $\Delta t$ , making it the equivalent of equation (19), but for the numerical algorithm. The ends of the curve conform to

the limits in equations (19) and (20), which are rewritten in reduced form:

$$\frac{k_{Ni} \Delta t}{\sigma_b^3} = 2\pi s^2, \quad \Delta t \rightarrow 0 \quad (26)$$

$$\frac{k_N \Delta t}{\sigma_b^3} = \frac{4\pi}{3}, \quad \Delta t \rightarrow \infty. \quad (27)$$

Thus, we have solved the forward problem, which is the solution of the rate constant that is actually simulated in terms of the simulation parameters. Since what is needed is a solution to the inverse problem, which is the binding radius that the simulation needs to use in order to reproduce a known reaction rate, an iterative search routine was written to invert the interpolated function. Using our *Smoldyn* program, we verified that irreversible bimolecular reaction rates are accurately simulated using a wide range of time steps.

#### 4.3. Reversible reactions

The reversible reaction  $A + B \leftrightarrow C$  has the additional complication of geminate recombinations. This topic is addressed on a general level before we derive reversible reaction rates for the Smoluchowski model and the numerical algorithm.

The probability of a geminate recombination is denoted by  $\phi$ . Of all the forward reactions that occur when the system is at equilibrium, which occur with reaction rate  $k_r$ , a fraction  $1 - \phi$  are non-geminate reactions. This portion of the reactants does not share a common history so all of their dynamics, including the rate at which they react ( $k_i$ ), are completely equivalent to the irreversible situation considered previously. This leads to a general relationship between the irreversible and reversible rate constants at equilibrium (true for the model, simulations and all physical systems):

$$k_i = (1 - \phi)k_r. \quad (28)$$

We are not suggesting that  $k_r$  is larger than  $k_i$  because of the physically unreasonable idea that reaction reversibility somehow makes molecules more reactive. Instead, if a reaction is reversible, the reactants are generated in close proximity to each other by the back reaction, which leads to faster reactant encounters and a higher reaction rate. The correct value for ‘the forward reaction rate constant’ depends on the conditions under which it was measured. If the experimental system was at equilibrium, then there must have been geminate reactions as well as non-geminate reactions, leading to the measurement of the larger reaction rate constant,  $k_r$ . On the other hand, if the product was removed as fast as it was formed, then there were no geminate reactions, leading to the measurement of the smaller irreversible rate constant,  $k_i$ . Below, we derive results for the equilibrium situation.

#### 4.4. Reversible reactions, Smoluchowski model

At equilibrium, the same number of A and B molecules are produced in back reactions as are lost in forward reactions, implying that the source of B molecules at  $\sigma_u$  exactly matches the sink at  $\sigma_b$ . This implies that there is no net flux of B towards

A molecules outside a distance  $\sigma_u$  and, to be consistent with zero flux and the boundary condition that  $g(\infty) = 1$ , the RDF must equal 1 for all  $r > \sigma_u$ . Equation (3) was solved using this modified boundary condition to yield the RDF for the Smoluchowski model for reversible reactions (figure 4(B)):

$$g_{Sr}(r) = 1 - \frac{\sigma_b(\sigma_u - r)}{r(\sigma_u - \sigma_b)}, \quad \sigma_b < r < \sigma_u. \quad (29)$$

As before, equation (17) yields the equilibrium rate constant. Combing the result with equation (28) yields the reversible reaction rate and the probability of geminate recombination:

$$k_{Sr} = \frac{k_{Si}}{1 - \phi_S} \quad (30)$$

$$\phi_S = \frac{\sigma_b}{\sigma_u}. \quad (31)$$

The latter result [12] confirms the statement made earlier that geminate rebinding in the model system becomes certain as  $\sigma_u$  is decreased to  $\sigma_b$ . It also has the intuitively reasonable property that  $\phi_S$  decreases to zero as  $\sigma_u$  is increased to infinity.

#### 4.5. Reversible reactions, numerical algorithm

The reaction rate for simulated reversible reactions was computed numerically in nearly the same manner as for irreversible reactions, although now for a series of  $\sigma'_u$  values, where  $\sigma'_u = \sigma_u/\sigma_b$ . While the unbinding radius cannot be less than the binding radius in the model system, there is no such restriction for the numerical algorithm, so these reduced reaction rates were computed as well. Back reactions were included in the rate computation by evaluating the flux of the RDF into the reduced binding radius with equation (25), and transferring it to the RDF at the reduced unbinding radius (figure 4(D)). Conceptually, this transferred flux forms a Dirac delta function at  $\sigma'_u$  after a reaction step. To improve numerical accuracy, the delta function was diffused separately and then added to the RDF one step later; a diffused delta function is simply  $\text{grn}(r, \sigma_u, s)$ . The reduced reaction rates are shown with light lines in figure 6. They represent  $k_{Nr}$  as functions of  $\sigma_b$ ,  $\sigma_u$  and  $s$ , making them the numerical algorithm equivalent of equation (30). Using an iterative search routine, the function was inverted to solve for the simulation parameters  $\sigma_b$  and  $\sigma_u$  from the experimentally known values  $k_r$  and  $\phi$ .

Errors in these data are estimated to be less than 2.1%. The numerical RDFs approached the analytical RDF in equation (29) for short time steps and the ends of the curves in figure 6 approach the limits found with equations (27) and (30).

#### 4.6. Bimolecular reactions with identical reactants

A final subtle point concerns the calculation of simulation parameters for reactions with the form  $A + A \rightarrow C$ . Using the methods given above, the simulated reaction rate turns out to be half as large as expected. The reason is that there are  $n_A n_B$  possible distinct collisions for the reaction  $A + B \rightarrow C$ , whereas there are only  $n_A(n_A - 1)/2$  distinct A–A collisions

for  $A + A \rightarrow C$  [36], where  $n_A$  and  $n_B$  are the total numbers of A and B molecules. Assuming the experimental reaction rate was measured with many reactant molecules, the factor  $n_A - 1$  simplifies to just  $n_A$ , leading to the factor of 2 of over-counting. The easiest correction method is to simply double all experimental rate constants for reactions with identical reactants before calculating simulation parameters.

## 5. Analysis of simulated dynamics

Using the binding and unbinding radii derived above, reaction rates with the bimolecular reaction algorithm will match experimentally determined reaction rates for any system at steady-state and using any length simulation time step. If the geminate recombination probabilities are known or can be guessed, simulation results will agree with them as well. However, away from steady-state, reaction rates differ slightly between reality and the model (the model treats all reactions as though they are diffusion limited) and between the model and the simulation. These issues are investigated here. It is shown that the errors frequently offset each other such that simulation results are actually closer to reality than the model is. We also find a way to estimate the geminate recombination probability from the reaction activation energy.

As seen in figure 4, the numerical RDF is discontinuous at the binding radius, unlike the model result, but suggestive of the RDF for the Collins and Kimball model [14, 17, 37]. This differs from the Smoluchowski model in that a reaction does not always occur when reactants collide, but occurs at a maximum reaction rate, as would arise from an activation barrier at the binding radius. To accomplish this, the statement that  $g_S(r) = 0$  at  $r = \sigma_b$  is replaced with the condition [29]:

$$\left. \frac{\partial g_C(r)}{\partial r} \right|_{\sigma_b} = \frac{g_C(\sigma_b)}{\gamma}. \quad (32)$$

The new subscript 'C' is used for the Collins and Kimball model; to be rigorous, both sides of the equation are evaluated at the limit of  $r \rightarrow \sigma_b^+$ . As mentioned previously, the physical picture is complicated because each A-B pair that collides once will almost certainly collide an infinite number of times, implying that the reaction probability at each individual collision is infinitesimal. Despite this, equation (3) can be solved with the new boundary condition to yield the steady-state RDF (figures 4(E) and (F)), the reaction rate constant for irreversible [14] and reversible reactions, and the probability of geminate recombination for reversible reactions:

$$g_{Ci}(r) = 1 - \frac{\sigma_b^2}{r(\sigma_b + \gamma)}, \quad r > \sigma_b \quad (33)$$

$$k_{Ci} = \frac{4\pi\sigma_b^2 D}{\sigma_b + \gamma} \quad (34)$$

$$g_{Cr}(r) = 1 - \frac{\sigma_b^2(\sigma_u - r)}{r(\sigma_u\gamma + \sigma_b\sigma_u - \sigma_b^2)}, \quad \sigma_b < r < \sigma_u \quad (35)$$

$$k_{Cr} = \frac{4\pi\sigma_b^2\sigma_u D}{\sigma_u\gamma + \sigma_b\sigma_u - \sigma_b^2} \quad (36)$$

$$\phi_C = \frac{\sigma_b^2}{\sigma_u(\sigma_b + \gamma)}. \quad (37)$$

The RDFs for the numerical algorithm are seen to be similar to those of the Collins and Kimball model (figure 4).

Suppose the reactants are maintained in a well-mixed state. This removes all diffusion effects from the reaction rate, making it limited only by the activation energy. In the Smoluchowski model, the discontinuity of this well-mixed RDF at  $\sigma_b$  implies an infinite slope at  $\sigma_b$  and an infinite reaction rate (using equation (17)). In contrast, the boundary condition of the Collins and Kimball model enforces a slope of  $1/\gamma$  at  $\sigma_b$  and thence the *activation-limited* rate constant for the Collins and Kimball model,

$$k_{Ca} = 4\pi\sigma_b^2 D\gamma^{-1}. \quad (38)$$

This rate constant is also called the intrinsic rate constant [37], with the loose interpretation that it is the reaction rate for a pair of molecules that are already in contact. Equations (36) and (38) are simplified to highlight the relationship between the Smoluchowski and Collins and Kimball models:

$$k_{Ci}^{-1} = k_{Si}^{-1} + k_{Ca}^{-1} \quad (39)$$

$$k_{Cr}^{-1} = k_{Sr}^{-1} + k_{Ca}^{-1}. \quad (40)$$

Along with the rest of the Collins and Kimball model, these reaction rates vary smoothly between the Smoluchowski description when  $\gamma \rightarrow 0$  and  $k_{Ca} \rightarrow \infty$ , to a well-mixed system when  $\gamma \rightarrow \infty$  and  $k_{Ca} \rightarrow 0$ . The Collins and Kimball model is a significant improvement to the Smoluchowski model because it can capture a whole range of reaction types, from diffusion limited to activation limited, while remaining fundamentally simple.

An analogous activation-limited rate constant is calculated for the numerical algorithm. A well-mixed RDF is diffused over one simulation time step with equation (21) and the reaction rate is found with equation (25) to yield

$$\begin{aligned} \frac{k_{Na}\Delta t}{\sigma_b^3} &= \frac{4\pi}{3} \left( \operatorname{erfc} \frac{\sqrt{2}}{s'} + s' \sqrt{\frac{2}{\pi}} \right) \\ &+ \frac{2\sqrt{2\pi}}{3} s' (s'^2 - 1) (e^{-2/s'^2} - 1). \end{aligned} \quad (41)$$

This result approaches infinity as  $\Delta t$  is reduced to zero and the simulation approaches the Smoluchowski model, while it becomes rate limiting with long time steps. Thus,  $\Delta t$  is a parameter in the numerical algorithm that adjusts the simulated dynamics from diffusion limited to activation limited, much as  $\gamma$  is a tunable parameter in the Collins and Kimball model.

The probabilities of geminate recombination form yet another similarity. From equation (37) and the model constraint that  $\sigma_u \geq \sigma_b$ ,  $\phi_C$  can decrease towards zero but cannot exceed  $\sigma_b/(\sigma_b + \gamma)$ . Similarly,  $\phi_N$  can be made arbitrarily small by using a large unbinding radius but it has a maximum value because the simulation  $\sigma_u$  cannot be decreased below zero. As with the activation-limited rate constants, the maximum  $\phi$  values depend on  $\gamma$  for the Collins and Kimball model and  $\Delta t$  for the numerical algorithm.

The upper limit on  $\phi_C$  can be used to address an issue that has been largely ignored up to this point: how is one supposed to choose the unbinding radius for a simulation? Using equation (28) and the curves in figure 6, it is possible to calculate the simulation parameters  $\sigma_b$  and  $\sigma_u$  from experimentally measured  $k_r$  and  $\phi$  values, provided that geminate recombination data can be found. Unfortunately, these data are nearly non-existent. A solution comes from the Collins and Kimball model in which it is physically most reasonable to set  $\sigma_u$  equal to  $\sigma_b$  and to limit the rate of geminate reactions with an activation barrier:

$$\phi_C = \frac{k_{Ca}}{k_{Ca} + k_{Si}}, \quad \sigma_u = \sigma_b. \quad (42)$$

The ‘C’ subscripts are retained here because the equation is only strictly accurate with the approximations of the Collins and Kimball model. However, the model is often a good description of physical systems, so the relationship is also likely to be reasonably accurate experimentally. If the activation-limited rate constant can be estimated, equation (42) yields  $\phi$ , which can then be used to find  $\sigma_u$  for a simulation.

Recall that a simulation can be interpreted as periodic observations of a virtual system that evolves continuously. Also, an exact bimolecular reaction algorithm would use the binding radius from the Smoluchowski model and would consider a reaction as having occurred between a pair of molecules if they had come closer than  $\sigma_b$  during a time step. Analogous exact algorithms can be imagined for the Collins and Kimball model or for any of several further improvements to these classic models [18, 34, 38, 39]. While the simulation does not reproduce any of them exactly, similarities with the Collins and Kimball model include the profile of the RDF, the activation energy and the geminate recombination probability. This suggests that the simulated dynamics, whether at steady-state or not, are likely to be reasonably consistent with the behavior that would be observed with the Collins and Kimball model. Of course, the simulation time step applies to every reaction in a simulated reaction network, so one cannot independently control the dynamics of multiple reactions. However, this is unlikely to have practical consequences because differences between steady-state and non-steady-state reaction rates are so small that they are very difficult to measure experimentally [32, 40].

## 6. Examples

### 6.1. Irreversible reaction

Our first example demonstrates that the algorithms can accurately simulate bimolecular reactions at and away from steady-state, using either diffusion-limited or activation-limited dynamics. It is based on a recent experiment on the kinetics of an acid–base reaction [32]. Starting with well-mixed acid (AH) and base (B) molecules, the experiment was initiated by photo-exciting the acid with a fast laser pulse. An irreversible proton transfer occurred when an excited acid molecule contacted a base molecule, with the reaction  $\text{AH} + \text{B} \rightarrow \text{A} + \text{BH}$ . Using transient fluorescence measurements

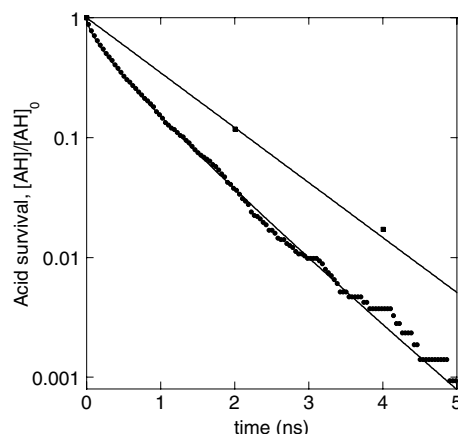


**Figure 7.** Progress of a bimolecular acid–base reaction that starts as a well-mixed system and approaches steady-state. The lower line is the non-exponential Smoluchowski solution for diffusion-limited dynamics (equation (43)) and the nearby solid circles are from a diffusion-limited simulation. Parameters:  $D_{\text{AH}} = 10^{-5} \text{ cm}^2 \text{ s}^{-1}$ ,  $D_{\text{B}} = 0$ , volume =  $10^6 \text{ nm}^3$ ,  $[\text{AH}]_0 = 3.3 \times 10^{-3} \text{ M}$  (2000 molecules),  $[\text{B}]_0 = 0.2 \text{ M}$  (120000 molecules),  $k_i = 5.3 \times 10^9 \text{ M}^{-1} \text{ s}^{-1}$ ,  $k_a = 5.1 \times 10^{10} \text{ M}^{-1} \text{ s}^{-1}$ ,  $\sigma_b = 0.73 \text{ nm}$ ,  $s = 0.063 \text{ nm}$ , and  $\Delta t = 0.002 \text{ ns}$  (only every 20th point is shown for clarity); runtime was 12 min on a Macintosh G4 laptop. The upper line is the exponential solution for activation-limited reactions (equation (44)) and the nearby solid squares are from a more nearly activation-limited simulation. Parameters are the same as before except  $k_a = 6.5 \times 10^9 \text{ M}^{-1} \text{ s}^{-2}$ ,  $\sigma_b = 1.81 \text{ nm}$ ,  $s = 2.0 \text{ nm}$ , and  $\Delta t = 2 \text{ ns}$ ; runtime was 4 s.

of the acid, the authors showed that the reaction progress was in close agreement with Smoluchowski dynamics (they included the Debye–Hückel corrections that are required for ionic species, although these had minimal effect due to high salt concentrations). Using similar parameters as those in the experiment, the lower line in figure 7 represents the analytically derivable Smoluchowski result [14]:

$$[\text{AH}] = [\text{AH}]_0 \exp \left[ -4\pi\sigma_b D[\text{B}]_0 \left( 1 + \frac{2\sigma_b}{\sqrt{\pi Dt}} \right) t \right]. \quad (43)$$

The curve has a very steep slope initially because the reactants start well-mixed; then, it flattens out to a straight line on the log-linear coordinates, as the system approaches steady-state. Using the same diffusion coefficients and steady-state reaction rate, the reaction was simulated with a very short time step to make the simulated dynamics diffusion limited. Agreement between theory and simulation is seen to be excellent at all times, although stochastic effects become apparent when there are few molecules.

The upper curve in figure 7 represents the theoretical behavior for an activation-limited reaction, using the same steady-state rate constant as before:

$$[\text{AH}] = [\text{AH}]_0 \exp(-k[\text{B}]_0 t). \quad (44)$$

Using a long time step, the same simulation algorithm accurately reproduced these activation-limited reaction dynamics as well.

Note that there are no adjustable parameters in either comparison. While it might be desirable to lower the time resolution of the former simulation and raise it for the latter one, this is impossible, because the length of the time step determines whether simulated dynamics are diffusion or activation limited. The diffusion-limited results satisfy the stated goal, which was that the observable simulation dynamics be as close as possible to the analytically derivable dynamics of the model system, while the activation-limited dynamics go an additional step, showing that it is also possible to simulate reactions that are not described by the Smoluchowski model.

## 6.2. Lotka–Volterra system

To demonstrate the value of stochastic spatial simulations, we turn to the canonical Lotka–Volterra system, which is a simple scheme that yields interesting dynamics. The reactions are [36]



The bar over the X indicates that its concentration is held constant. The system was introduced independently by Lotka and Volterra as ecological models [41]:  $Y_1$  is a prey species that multiplies after feeding on X, and  $Y_2$  is a predator species that multiplies after feeding on the prey  $Y_1$ . Analysis reveals stable oscillations in the concentrations of  $Y_1$  and  $Y_2$  as well as a neutrally stable stationary solution:

$$Y_1 = \frac{c_3}{c_2}, \quad Y_2 = \frac{c_1 \bar{X}}{c_2}. \quad (46)$$

Using a simulation method that accounts for stochastic effects but not space, Gillespie showed that the stochastic behavior of these reactions is quite different from deterministic results [36]. In particular, the system does not remain at the stationary point, but develops regular oscillations with a widely varying amplitude (dashed lines in figure 8(A)).

These reactions were simulated with the algorithms presented here using the same rate constants and initial condition, and with the  $Y_1$  and  $Y_2$  molecules distributed randomly initially. Rather than including X molecules explicitly, the first reaction was simulated as a unimolecular reaction with a rate constant  $c_1 X = 10$ . Spontaneous pattern formation emerged just after the simulation began, one snapshot of which is shown in figure 8(B). This led to dynamics that are markedly different from those found with either deterministic results or the Gillespie algorithm. In the spatial simulation, the oscillations are less regular, transitions are sharper, and there are occasional extreme deviations away from the steady-state solution. Many of these behaviors have been seen before, although most prior results used continuously variable reactant concentrations and/or a discrete spatial lattice [42–44]. Thus, with each level of detail that is added to a simulation, including first stochastics and then space, there can be large effects on the resulting dynamics of the system as a whole.

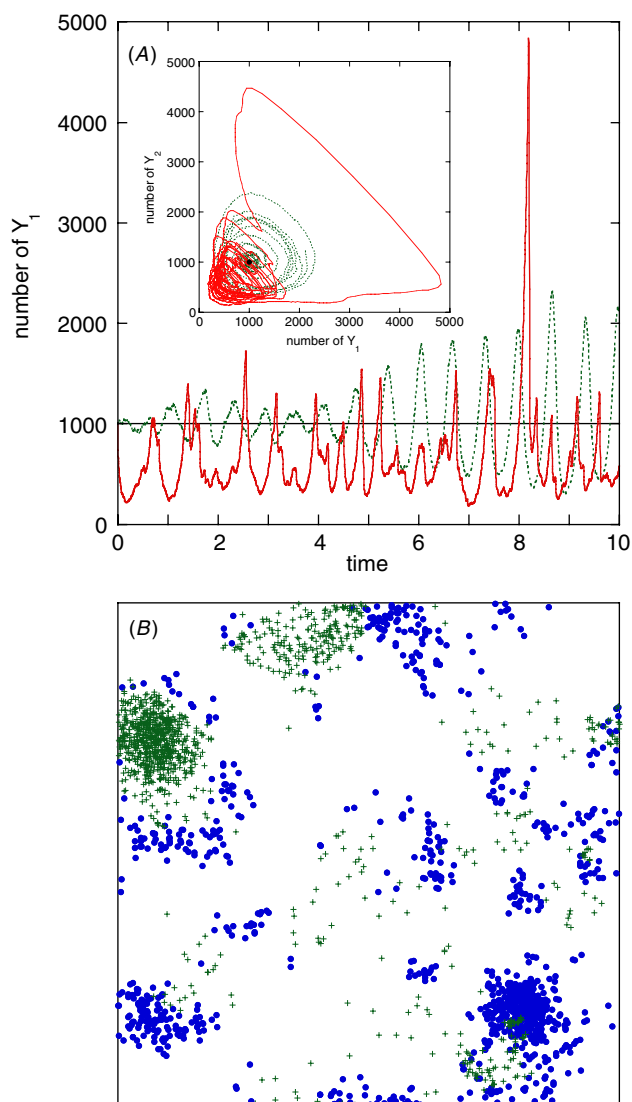


**Figure 8.** Dynamics of a Lotka–Volterra system. (A) Time course of the number of  $Y_1$  molecules shown with three different models. The black line at  $Y_1 = 1000$  is the deterministic solution for the neutrally stable stationary point; the green dashed line, created with the Gillespie algorithm, includes stochasticity but no spatial information; the red solid line, created with the algorithms presented here, includes both stochasticity and spatial detail. Note that the behaviors are quite different for the three models, demonstrating the value of the higher level of detail. Inset: a phase space portrait of the data shown in the time series using the same line styles; the deterministic solution is a point at  $Y_1 = Y_2 = 1000$ . (B) A snapshot of the spatial simulation shown in the previous panels, with blue dots for  $Y_1$  molecules and green '+' symbols for  $Y_2$ . This image was taken at time 2.6, which was during a sharp decline of  $Y_1$  and a growth of  $Y_2$ , where most of this activity is occurring in the upper left corner of the image. The high degree of pattern formation emerged spontaneously from a nearly homogeneous initial state and was very transient. Reaction parameters:  $X = 10^5$ ,  $c_1 = 0.0001$ ,  $c_2 = 0.01$ ,  $c_3 = 10$ , and initial values are  $Y_1 = Y_2 = 1000$ . Simulation parameters: volume dimensions are 200 on  $x$  and  $y$ , and 20 on  $z$ , with periodic boundaries, 10 units of time were simulated in steps of 0.001 time units, and diffusion constants are 100 for each  $Y_1$  and  $Y_2$ , leading to rms step lengths of 0.447. The  $Y_1 + Y_2$  reaction was simulated with  $\sigma_b = 3.55$ . Runtime was 70 s.

## 7. Conclusions and outlook

The algorithms presented here allow the accurate simulation of reaction networks with the inclusion of the stochasticity that arises from the discreteness of molecules and with spatial detail that can be accurate down to near the size scale of individual molecules. Simulation algorithms for diffusion, surface interactions and zeroth- and first-order reactions could be made exact, meaning that simulation results were shown to match the analytical results of an idealized model system using any length simulation time step. However, long time steps lead to discrepancies when different processes are coupled together. Bimolecular reactions were made as efficient as possible using the rule that two molecules react whenever they are found to be within their binding radius at the end of a time step. This parameter is calculated from the steady-state reaction rate constant and the simulation time step using the data in figure 6, yielding reaction rates that are exact when the system is at steady-state and are reasonably accurate at other times. The simulated reaction dynamics are similar to those of a Collins and Kimball type model and, likewise, can be characterized as diffusion or activation limited.

The examples demonstrate that these simulation algorithms work well in practice. Bimolecular reaction rates are simulated accurately at and away from steady-state with either activation- or diffusion-limited dynamics. Various levels of simulation detail with the Lotka–Volterra reactions demonstrate that the overall dynamics of a system of coupled reactions can be sensitive to stochastic and spatial effects. The algorithms run quickly enough that these examples were simulated on a laptop computer in several minutes.

These algorithms open up new avenues of research, allowing simulation detail at a level that was previously unattainable. They fill a gap between the more accurate and very computationally intensive molecular dynamics calculations, and the much coarser differential equation based reaction–diffusion methods. They are likely to be most useful for systems with several thousand molecules and with complex spatial constraints. For example, our *Smoldyn* program is currently being used to examine the diffusion and reaction of signaling molecules in the *E. coli* chemotaxis pathway, including effects from intracellular macromolecular crowding [23]. We also used these methods to investigate the repeated bindings of a single ligand to a cluster of receptors [24].

An additional algorithm that would be useful is one for simulations of molecule–fiber interactions, because that would allow studies of polymer growth, microtubule dynamics, DNA transcription and RNA translation, to name but a few examples. With this addition, and perhaps a few others, it should be possible to simulate essentially any biochemical process using individual molecules and a high level of spatial resolution. At that point, the hurdles to simulating an entire bacterium are computational power and experimentally determined inputs for the simulation.

*Supporting information.* Implementation of the bimolecular reaction algorithm presented here requires a look-up table for the data shown in figure 6. These data are available via the Internet at the *Physical Biology* website at <http://www.iop.org/EJ/journal/physbio>. They are presented in tabular form and in the code of several C language routines. The routines

execute data interpolation, extrapolation and tabular inversion so as to yield simulation parameters from experimental values. The C code that was used to generate the data table is included as well. The *Smoldyn* executable program, source code, and sample input files are available at the author’s website: <http://sahara.lbl.gov/~sandrews/software.html>.

## Acknowledgments

This work was funded by NIGMS grant GM64713, the Genomes to Life Project of the US Department of Energy, and by an NSF postdoctoral fellowship in biological informatics awarded to SSA. Comments on the manuscript by Dan Gillespie and Tom Shimizu are appreciated, as is assistance from Adam Arkin.

## Appendix. Implementation details

### A.1. Diffusion

In the diffusion algorithm, a uniformly distributed random number is converted to a normally distributed number for each spatial dimension, for each molecule, and at every time step. The Box–Muller transformation [35] is easy to implement but the required trigonometric calculations make this heavily used algorithm run slowly. Instead, the use of a look-up table is nearly as accurate and runs much faster. To create an  $n$  element look-up table, indexed from 0 to  $n - 1$ , the  $i$ th element is

$$X_i = \sqrt{2} \operatorname{erf}^{-1} \left( \frac{2i + 1}{n} - 1 \right). \quad (\text{A1})$$

If  $i$  is a random integer between 0 and  $n - 1$ ,  $X_i$  is a normally distributed random variable with standard deviation 1, and  $\sigma X_i$  is the desired normal deviate with mean 0 and standard deviation  $\sigma$ . This equation is derived by integrating a Gaussian probability density with unit variance to yield an error function and then inverting the result [35]. A table is not quite as accurate as an analytical transformation because there are typically fewer table entries than available random numbers although this is not a significant constraint for Brownian dynamics because the number of possible displacements for each molecule is the cube of the number of table entries for a three-dimensional system with one time step, and increases exponentially with additional time steps.

### A.2. Surface interactions

Surface interactions are sufficiently easy to simulate that they are described in the main text. The one exception is that spatial partitions, described below, can be used to minimize the number of molecule–surface interactions that need to be checked.

### A.3. Zeroth-order reactions

During one time step, the probability that exactly  $j$  molecules of type A are produced is given with a Poisson distribution [28]:

$$\operatorname{Prob}(j) = \frac{(k_0 \Delta t)^j \exp(-k_0 \Delta t)}{j!}. \quad (\text{A2})$$

This can be computed easily with a rejection method [35]. Some computational efficiency can be gained by calculating the required probabilities during program initialization and storing them in look-up tables (one for each zeroth-order reaction). However, the overall improvement in speed is typically negligible because only one Poisson deviate is required for each zeroth-order reaction at each time step.

#### A.4. Unimolecular reactions

Rather than re-calculating the reaction probabilities given in equation (14) at each time step, it is faster to calculate them just once for each possible unimolecular reaction during program initialization. Additional computational efficiency is gained by summing these probabilities. Using  $i$  as an index for a pathway by which a molecule can undergo a unimolecular reaction, the reaction probabilities for pathway 1 to  $i$  are summed to form a list of cumulative reaction probabilities. At each time step during the simulation, a specific molecule reacts by pathway  $i$  if a uniform deviate is less than the  $i$ th stored cumulative probability value and greater than the preceding value.

#### A.5. Bimolecular reactions

Although it complicates the implementation, spatially partitioning the simulation volume [10, 45] is essential to reduce the proportionality of the runtime for bimolecular reactions from second order in the total number of molecules to first order. To do this, the program maintains a separate list of the molecules for each region. When checking for bimolecular reactions, the program only needs to investigate pairs of molecules that are in the same or neighboring regions. In the same way, partitions also speed up the simulation of surface interactions.

#### A.6. Simulation time step

Discrepancies between the simulated dynamics and those of the model system arise from the following: spatial resolution that cannot exceed the rms step length (figure 1), bimolecular reaction dynamics that are closer to the Collins and Kimball model than the Smoluchowski model, and the coupling of molecular processes. The last error is very difficult to analyze, so we present a practical rule-of-thumb instead. A simulation is run with a trial time step that is short enough to yield the needed spatial resolution and again with a time step that is half as long. The longer time step is short enough if the results between the two runs are essentially the same (recalling that they will always differ somewhat due to stochasticity); otherwise, the time step needs to be reduced. This works because all errors decrease monotonically with smaller simulation time steps.

## Glossary

*Activation limited.* Chemical reactions in which the reaction rate is fully determined by an activation energy barrier, making the reactant diffusion coefficients unimportant.

*Binding radius.* The separation at which a pair of reactant molecules react.

*Brownian dynamics.* A simulation method for molecular diffusion in which each molecule takes a step chosen from a Gaussian distribution, at each time step.

*Brownian motion.* Diffusive motion of a molecule that has been idealized to obey Fick's laws at all size and time scales, leading to an infinitely detailed trajectory.

*Collins and Kimball model.* An extension of the Smoluchowski model that includes an activation energy barrier for bimolecular reactions.

*Diffusion influenced.* Chemical reactions in which reactant diffusion is slow enough to influence the reaction rate.

*Diffusion limited.* Chemical reactions in which reactant diffusion is so slow that it completely determines the reaction rate.

*Geminate recombination.* The reaction of a pair of product molecules that were created from the same reactant molecule, back to yield a reactant.

*Mutual diffusion coefficient.* The sum of the diffusion coefficients for two reactants.

*Mutual rms step length.* The rms step length that is calculated from a mutual diffusion coefficient.

*Radial distribution function (RDF).* The distribution of distances between individual molecules of one type and those of another type, averaged over every pair of molecules.

*Root mean square (rms) step length.* The average length of a step for a molecule in a Brownian dynamics simulation.

*Smoldyn.* A general purpose stochastic spatial simulation program that incorporates all the algorithms described here.

*Smoluchowski model.* An analytical model of chemical reactions in which spherical molecules react upon collision.

*Steady-state.* A situation in which neither the spatial correlation of reactants nor the bimolecular reaction rate constant changes over time.

*Unbinding radius.* The initial separation between a pair of products of a reversible reaction, introduced to reduce the probability of back reactions.

*Well mixed.* A situation in which reactant molecules are mixed uniformly throughout the simulation volume; the only spatial correlation is that reactants do not overlap each other.

## References

- [1] Arkin A P 2001 *Curr. Opin. Biotechnol.* **12** 638
- [2] Slepchenko B M, Schaff J C, Carson J H and Loew L M 2002 *Annu. Rev. Biophys. Biomol. Struct.* **31** 423
- [3] Takahashi K *et al* 2002 *IEEE Intell. Syst.* **17** 64
- [4] Barkai N and Leibler S 1997 *Nature* **387** 913

- [5] Levin M D, Morton-Firth C J, Abouhamad W N, Bourret R B and Bray D 1998 *Biophys. J.* **74** 175
- [6] Duke T A J, LeNovère N and Bray D 2001 *J. Mol. Biol.* **308** 541
- [7] Ryan K R and Shapiro L 2003 *Annu. Rev. Biochem.* **72** 367
- [8] Kholodenko B N, Brown G C and Hoek J B 2000 *Biochem. J.* **350** 901
- [9] Rao C V, Wolf D M and Arkin A P 2002 *Nature* **420** 231
- [10] Stiles J R and Bartol T M 2001 Monte Carlo methods for simulating realistic synaptic microphysiology using MCell *Computational Neuroscience: Realistic Modeling for Experimentalists* ed E De Schutter (Boca Raton, FL: CRC Press)
- [11] von Smoluchowski M V 1917 *Z. Phys. Chem.* **92** 129
- [12] Berg H C 1993 *Random Walks in Biology* 2nd edn (Princeton, NJ: Princeton University Press)
- [13] Elowitz M B, Surette M G, Wolf P-E, Stock J B and Leibler S 1999 *J. Bacteriol.* **181** 197
- [14] Rice S A 1985 *Diffusion Limited Reactions (Comprehensive Chemical Kinetics vol 25)* ed C H Bamford, C F H Tipper and R G Compton (Amsterdam: Elsevier)
- [15] Schnell S and Turner T E 2004 *Prog. Biophys. Mol. Biol.* **85** 235
- [16] Northrup S H and Erickson H P 1992 *Proc. Natl Acad. Sci. USA* **89** 3338
- [17] Collins F C and Kimball G E 1949 *J. Colloid Sci.* **4** 425
- [18] Agmon N 1984 *J. Chem. Phys.* **81** 2811
- [19] Berlin Y A, Cordier P and Delaire J A 1980 *J. Chem. Phys.* **73** 4619
- [20] Noyes R M 1955 *J. Am. Chem. Soc.* **77** 2042
- [21] Atkins P W 1986 *Physical Chemistry* 3rd edn (New York: Freeman)
- [22] Northrup S H and Hynes J T 1980 *J. Chem. Phys.* **73** 2700
- [23] Lipkow K, Andrews S S and Bray D 2004 *J. Bacteriol.* at press
- [24] Andrews S S and Bray D 2004 in preparation
- [25] Crank J 1975 *The Mathematics of Diffusion* 2nd edn (Oxford: Oxford University Press)
- [26] Edelman A L and Agmon N 1993 *J. Chem. Phys.* **99** 5396
- [27] Ermak D L and McCammon J A 1978 *J. Chem. Phys.* **69** 1352
- [28] Snell J L 1988 *Introduction to Probability* (New York: Random House)
- [29] Carslaw H S and Jaeger J C 1959 *Conduction of Heat in Solids* 2nd edn (Oxford: Clarendon)
- [30] Zon J S v and Wolde P R T 2004 *Preprint q-bio. MN/0404002*
- [31] Stundzia A B and Lumsden C J 1996 *J. Comput. Phys.* **127** 196
- [32] Cohen B, Huppert D and Agmon N 2000 *J. Am. Chem. Soc.* **122** 9838
- [33] McQuarrie D A 2000 *Statistical Mechanics* (Sausalito, CA: University Science Books)
- [34] Szabo A 1989 *J. Phys. Chem.* **93** 6929
- [35] Press W H, Flannery B P, Teukolsky S A and Vetterling W T 1988 *Numerical Recipes in C. The Art of Scientific Computing* (Cambridge, UK: Cambridge University Press)
- [36] Gillespie D T 1977 *J. Phys. Chem.* **81** 2340
- [37] Hynes J T 1985 The theory of reactions in solution *Theory of Chemical Reaction Dynamics* ed M Baer (Boca Raton, FL: CRC Press)
- [38] Weaver D L 1980 *J. Chem. Phys.* **72** 3483
- [39] Popov A V and Agmon N 2001 *J. Chem. Phys.* **115** 8921
- [40] Sikorski M, Krystkowiak E and Steer R P 1998 *J. Photochem. Photobiol. A* **117** 1
- [41] Boyce W E and DiPrima R C 1992 *Elementary Differential Equations* 5th edn (New York: Wiley)
- [42] Vilar J M G and Solé R V 1998 *Phys. Rev. Lett.* **80** 4099
- [43] Spagnolo B and Barbera A L 2002 *Physica A* **315** 114
- [44] Satulovsky J E and Tomé T 1997 *J. Math. Biol.* **35** 344
- [45] Frenkel D and Smit B 2002 *Understanding Molecular Simulation: from Algorithms to Applications* 2nd edn (San Diego, CA: Academic)